remote sensing

MDPI

Article

Haze Optical Properties from Long-Term Ground-Based Remote Sensing over Beijing and Xuzhou, China

Kai Qin [1,*], Luyao Wang [1], Jian Xu [2], Husi Letu [3,*], Kefei Zhang [1,4], Ding Li [1], Jiaheng Zou [1] and Wenzhi Fan [1]

1 School of Environment Science and Spatial Informatics, China University of Mining and Technology, Xuzhou 221116, China; luyaowang92@163.com (L.W.); lidinf@cumt.edu.cn (D.L.); zoujiaheng@cumt.edu.cn (J.Z.); fwzcumt@163.com (W.F.)
2 German Aerospace Center, Remote Sensing Technology Institute, 82234 Weßling, Germany; jian.xu@dlr.de
3 Institute of Remote Sensing and Digital Earth, Chinese Academy of Sciences, Beijing 100864, China
4 School of Science, RMIT University, Melbourne VIC 3000, Australia; kefei.zhang@rmit.edu.au
* Correspondence: qinkai@cumt.edu.cn or qinkai20071014@163.com (K.Q.); husiletu@radi.ac.cn (L.H.); Tel.: +86-159-5066-3287 (K.Q.)

Received: 22 January 2018; Accepted: 23 March 2018; Published: 26 March 2018

Abstract: Aerosol haze pollution has had a significant impact on both global climate and the regional air quality of Eastern China, which has a high proportion of high level pollution days. Statistical analyses of aerosol optical properties and direct radiative forcing at two AERONET sites (Beijing and Xuzhou) were conducted from 2013 to 2016. Results indicate: (1) Haze pollution days accounted for 26% and 20% of days from 2013 to 2016 in Beijing and Xuzhou, respectively, with the highest proportions in winter; (2) The averaged aerosol optical depth (AOD) at 550 nm on haze days were about 3.7 and 1.6 times greater than those on clean days in Beijing and Xuzhou, respectively. At both sites, the maximum AOD occurred in summer; (3) Hazes were dominated by fine particles at both sites. However, as compared to Xuzhou, Beijing had larger coarse mode AOD and higher percentage of small α. This data, together with an analysis of size distribution, suggests that the hazes in Beijing were more susceptible to coarse dust particles than Xuzhou; (4) During hazes in Beijing, the single scattering albedo (SSA) is significantly higher when compared to clean conditions (0.874 vs. 0.843 in $SSA_{440\,nm}$), an increase much less evident in Xuzhou. The most noticeable differences in both SSA and the imaginary part of the complex refractive index between Beijing and Xuzhou were found in winter; (5) In Beijing, the haze radiative forcing produced an averaged cooling effect of -113.6 ± 63.7 W/m^2 at the surface, whereas the averaged heating effect of 77.5 ± 49.7 W/m^2 within the atmosphere was at least twice as strong as clean days. In Xuzhou, such a radiative forcing effect appeared to be much smaller and the difference between haze and clean days was insignificant. Derived from long-term observation, these findings are more significant for the improvement of our understanding of haze formation in China and the assessment of its impacts on radiative forcing of climate change than previous short-term case studies.

Keywords: haze; aerosol; optical properties; statistical analyses; AERONET; China

1. Introduction

Although atmospheric aerosols play a significant and complex role in Earth's radiation energy budget through direct and indirect effects [1], they are also associated with public health problems [2]. Varying temporally and spatially, aerosols' optical and physical properties are crucial parameters that influence the aerosol radiative forcing both at the surface/bottom and at the top of atmosphere; these parameters include the aerosol optical depth (AOD), Ångström exponent (α), the single

scattering albedo (SSA), aerosol size distribution, and complex refractive index. Ground-based Sun-sky radiometer networks have been widely established to provide long-term global/regional measurements of these aerosol properties, such as the AErosol RObotic NETwork (AERONET) [3], PHOtométrie pour le Traitement Opérationnel de Normalisation Satellitaire (PHOTONS) [4], China Aerosol Remote Sensing Network (CARSNET) [5], and SKY radiometer NETwork (SKYNET) [6]. Several research activities on aerosol optical properties and associated radiative forcing effects have been reported through the use of ground-based remote sensing data [7–17].

China has experienced rapid industrialization and urbanization over the last decades, resulting in heavy aerosol loadings. Notably, frequent haze episodes with record-breaking $PM_{2.5}$ (atmospheric particulate matter with a diameter of 2.5 μm or less) loading level have occurred over eastern China [18–22]. This has attracted increased attention with respect to the reliable analysis of aerosol optical properties under these haze conditions in China. Li et al. [23] used a Sun-sky radiometer to retrieve aerosol optical, physical, and chemical characterization during two haze episodes in the winters of 2011 and 2012 in Beijing. Bi et al. [24], Che et al. [25], and Yu et al. [26] studied several heavy haze pollution episodes in Beijing in January 2013. Furthermore, Che et al. [27] studied Sun-sky radiometer measurements at seven sites over rural, suburban, and urban regions of the North China Plain in January 2013. Qin et al. [28] investigated the prolonged hazes in the winter from late 2013 to early 2014 in Shijiazhuang. Kang et al. [29] gave the variations of aerosol optical properties on a haze day of 12 June 2008 in Nanjing. Zhang et al. [30] analyzed aerosol optical properties and calculated aerosol radiative forcing during a haze period from 25 December 2015 to 18 January 2016 in Wuhan.

However, most of the research mentioned above focus on case studies during short-term haze episodes. The main objective of this paper is to provide a long-term statistical study of haze optical properties in China. There are only six long-term AERONET sites in eastern China providing long-term data beginning in 2013 ($PM_{2.5}$ data was not freely available in China before 2013), i.e., Beijing, Beijing-RADI, Beijing-CAMS, XiangHe, Xuzhou-CUMT, and Taihu. Four of these six sites are in Beijing and its surrounding areas. The XiangHe site is in a rural area, approximately 65 km away from downtown Beijing. The Taihu site is close to the Taihu Lake. Given that the haze is found predominantly in urban regions, the two sites of Beijing-RADI and Xuzhou-CUMT were chosen. Additionally, aerosol radiative forcing was calculated using the Santa Barbara DISORT Atmospheric Radiative Transfer (SBDART) model.

2. Data and Method

2.1. Sites and Measurements

The two AERONET sites used in the study, Beijing-RADI and Xuzhou-CUMT, are in downtown Beijing and suburban Xuzhou, respectively. Both Beijing and Xuzhou are part of generalized North China Plain (NCP) that is bordered to the north by the Yanshan Mountains, to the west by the Taihang Mountains, and to the east by both the Bohai Sea and Yellow Sea (see Figure 1). The NCP is one of the most polluted regions in China. The Beijing-RADI site at the Institute of Remote Sensing and Digital Earth, Chinese Academy of Sciences (40.005°N, 116.379°E, 59 m), is in the northern part of Beijing, between the 4th and 5th city ring roads. The predominant types of land use around the site are roads and residential areas. The Xuzhou-CUMT site at the China University of Mining and Technology (34.220°N, 117.140°E, 60 m), is surrounded by mountains on three sides as well as a lake on its northern side. The predominant types of land use around this site are roads and residential areas. There are three levels of AERONET data [31]. The dataset used for the Beijing-RADI was taken from the Version 2 Level 2 (quality assured) products with observations from January 2013 to December 2016. The dataset for the Xuzhou-CUMT was taken from the Level 1.5 (cloud screened) product with observations from July 2013 to December 2016.

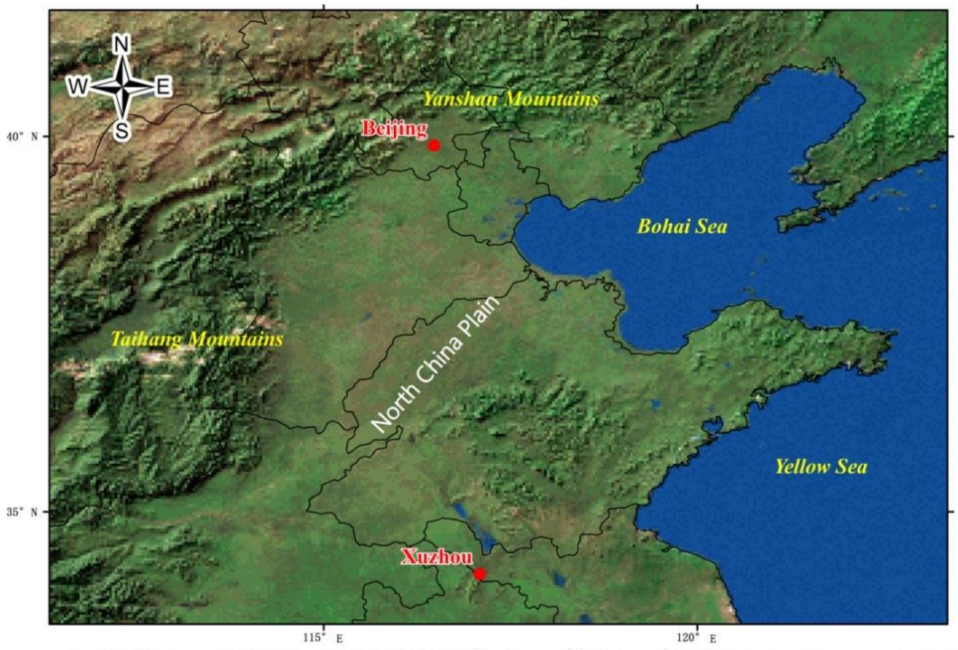

Figure 1. Elevation map of the North China Plain plotted using ArcGIS software based on the Shuttle Radar Topography Mission 90 m digital elevation data [32]. Red points indicate the location of Beijing and Xuzhou sites which are the only two urban sites with long-term measurements provided by the AERONET.

The automatic Sun-sky radiometer scans direct solar irradiance four times an hour at eight spectral channels (340, 380, 440, 500, 675, 870, 1020, and 1640 nm) and a 940 nm water vapor channel with a 1.2° full field of view. The measurements of direct solar irradiance for each band can be employed to calculate the AOD and the measurements at 940 nm are capable of computing total perceptible water vapor content in centimeters. The uncertainty in AOD retrievals under cloud free conditions is $<\pm 0.02$ for the channel with central wavelength of 440 nm and $<\pm 0.01$ for other channels, which is less than the $\pm 5\%$ uncertainty for the retrievals of sky radiance measurements [33]. The α is estimated at two wavelengths of 870 nm and 440 nm which is commonly used to describe the wavelength dependence of AOD and to provide some basic information on aerosol size distribution. Small values of α correspond to the predominant presence of coarse and large values of α of fine aerosol particles. A spectral deconvolution algorithm was developed to infer the component fine and coarse mode optical depths at 500 nm from the spectral total extinction AOD data based on two fundamental assumptions [34]. The first is that the aerosol particle size distribution is effectively bimodal. The second hypothesis is that the coarse-mode α and its spectral variation are both approximately neutral. The SSA and aerosol size distribution, together with the complex refractive index and the aerosol phase function, are simultaneously retrieved by using both sky radiance almucantar measurements and direct solar measurements at four wavelengths (440, 675, 870, and 1020 nm) [35]. The uncertainty of SSA ranges between 0.03 and 0.05, depending on the aerosol type and loading. Retrieval errors of volume size distribution typically do not exceed 10% for the intermediate particle size range ($0.1\ \mu m \leq r \leq 7\ \mu m$) and may greatly increase at the edges of the range ($r > 0.1\ \mu m$ or $r < 10\ \mu m$) [36].

2.2. Auxiliary Data

In May 2014, the Chinese Ministry of Environmental Protection drafted definitions for the conditions that qualify a day as having haze pollution (Technical regulation for haze pollution day judging (on trial)). The primary indicator of haze pollution is $PM_{2.5}$. A haze pollution day occurs when the average concentration of $PM_{2.5}$ is above 75 micrograms per cubic meter and visibility is less than 5km for more than six consecutive hours due to an increasing concentration of fine particulate

matters. Accordingly, $PM_{2.5}$ and visibility data were used to determine haze pollution days (HPDs). For Beijing, the hourly $PM_{2.5}$ data was obtained from the National Real-Time Air Quality Reporting System [37] and the hourly visibility data was acquired from the website designed and supported by Raspisaniye Pogodi Ltd., St. Petersburg, Russia [38]. For Xuzhou, the hourly $PM_{2.5}$ and visibility data were measured by an aerosol particle analyzer (model Grimm 180) and a visibility sensor (model Belfort Model 6000) equipped at the air quality monitoring site of China University of Mining and Technology. Additionally, the hourly relative humidity data in Xuzhou was measured by a weather station (model Vantage Pro 2).

2.3. Estimation of Aerosol Radiative Forcing

The direct aerosol radiative forcing (DARF) is defined as the difference between the net (down minus up) shortwave radiation fluxes (in W/m^2) with and without aerosols under cloud free conditions, indicating the rate at which the atmosphere is forced per unit of AOD. In this study, we determined the shortwave (0.3–4.0 μm) DARF using the SBDART model that was developed to calculate the solar radiations both within the Earth's atmosphere and at the surface under clear and cloudy conditions [39]. The key input parameters to run the model include the spectral values of AOD, SSA, asymmetry along with α, columnar water vapor content, total ozone amount, and spectral surface albedo. The aerosol optical parameters were from Sun-sky radiometer measurements in Beijing and Xuzhou AERONET sites. The total column ozone concentration and surface albedo values were obtained from the OMI and MODIS satellite datasets through the Giovanni online data system, developed and maintained by the NASA GES DISC [40]. Although the AERONET also provided the DARF data, calculated using similar radiative transfer equation, the SBDART has been more widely verified with surface broadband spectrum irradiance observations [41].

3. Results and Discussion

3.1. Occurrences of Haze Pollution Days

According to the Chinese Ministry of Environmental Protection's criteria, the total numbers of HPDs from 2013 to 2016 in Beijing and Xuzhou were 377 and 292, respectively, indicating a higher occurrence in Beijing. From 2013 to 2016, the frequency of HPDs exhibited a decreasing trend in Xuzhou, whereas it maintained a high level in Beijing, especially in 2014 (Figure 2). Figure 3 shows monthly variations of HPDs numbers in Beijing and Xuzhou. The highest proportions were found in winter months (December, January, and February), with more than one-third in Beijing and half in Xuzhou, respectively. Beijing had higher occurrences of HPDs than Xuzhou in spring, summer, and fall months except for June, while Xuzhou had more HPDs in winter months. Frequent straw burning episodes in Xuzhou and its surrounding areas account for the high level of HPDs in the area in June [42].

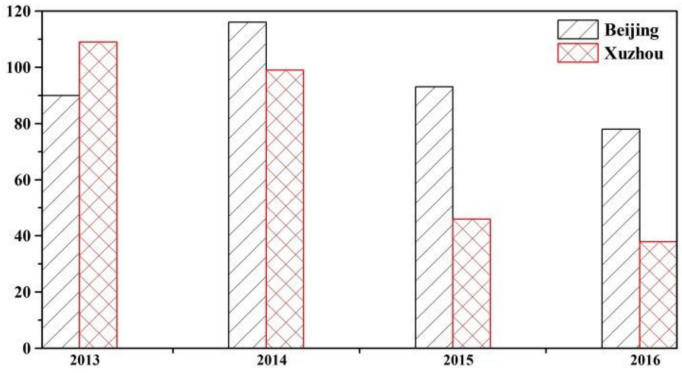

Figure 2. Number of haze pollution days in Beijing and Xuzhou between 2013 and 2016. A haze pollution day is a day with the average concentration of $PM_{2.5}$ above 75 micrograms per cubic meter and visibility below 5 km for more than six consecutive hours.

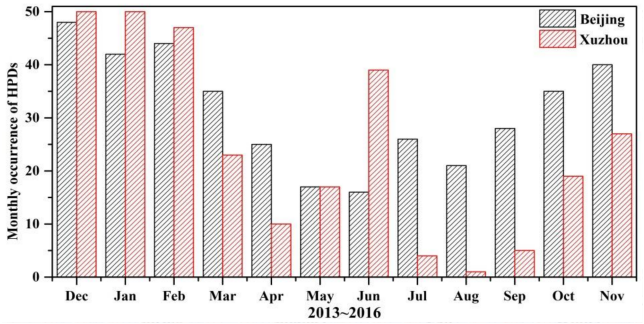

Figure 3. Monthly occurrence of haze pollution days in Beijing and Xuzhou between 2013 and 2016.

3.2. AOD and Ångström Exponent

Averaged AODs at different wavelengths on HPDs and non-haze pollution days (NHPDs) in Beijing and Xuzhou from 2013 to 2016 are shown in Figure 4. Generally, the AOD decreased in contrast to an increase in wavelength, especially on HPDs. This dependence of the AOD on wavelength is consistent with other research, e.g., Adeyewa and Balogun [43] and Wang et al. [44].The AOD on HPDs was evidently larger than those on NHPDs. The mean magnitudes of $AOD_{500\,nm}$ on HPDs were about 3.7 and 1.6 times greater than those on NHPDs in Beijing and Xuzhou, respectively. On HPDs, the values in Beijing and Xuzhou were similar. However, Xuzhou had near two times larger AOD than Beijing on HPDs, showing a higher background level of aerosol loading.

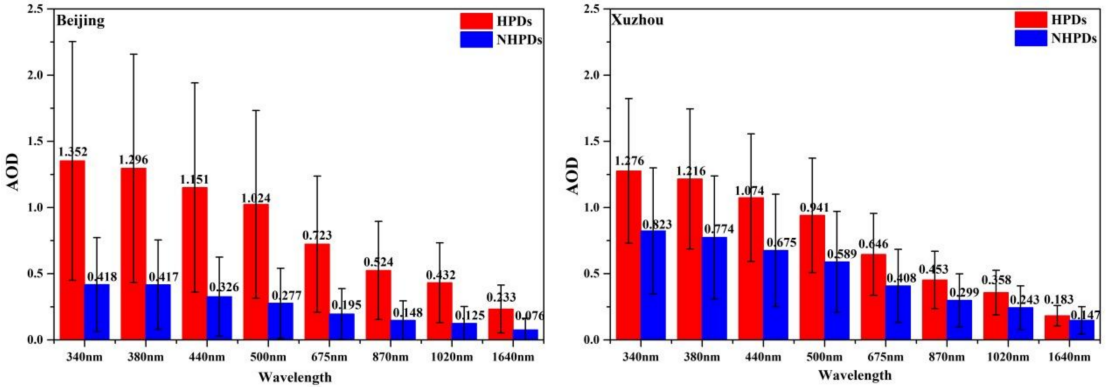

Figure 4. Averaged aerosol optical depth (AOD) at eight wavelengths on haze pollution days (HPDs) and non-haze pollution days (NHPDs) between 2013 and 2016 in Beijing and Xuzhou, respectively.

A seasonal comparison in Figure 5 reveals that the maximum AOD occurred in summer at both sites; however, the highest proportion of HPDs occurred in winter, as shown in Figure 3. This could be the case because: (1) aerosols can easily absorb moisture, grow, and finally increase the AODs with large water vapor contents in summer [45]; (2) high temperatures in summer are favorable to the formation of secondary aerosol particles [46]. In contrast, all the AODs in Beijing in spring, summer, and fall were larger than those in Xuzhou. However, Xuzhou had a larger AOD in winter than Beijing (0.882 vs. 0.621), which could be attributed to the higher number of HPDs.

Fine and coarse modes $AOD_{500\,nm}$ and fine-mode fraction (FMF, denoted as fine mode $AOD_{500\,nm}$ divided by total $AOD_{500\,nm}$) on HPDs and NHPDs in Beijing and Xuzhou from 2013 to 2016 are presented in Figure 6. The mean FMF on HPDs were 0.778 ± 0.209 and 0.882 ± 0.093 in Beijing and Xuzhou, indicating that haze pollutions were dominated by fine particles. The coarse mode $AOD_{500\,nm}$ on HPDs was about 1.6 times larger than that on NHPDs in Beijing in contrast to a factor of 0.8 in Xuzhou.

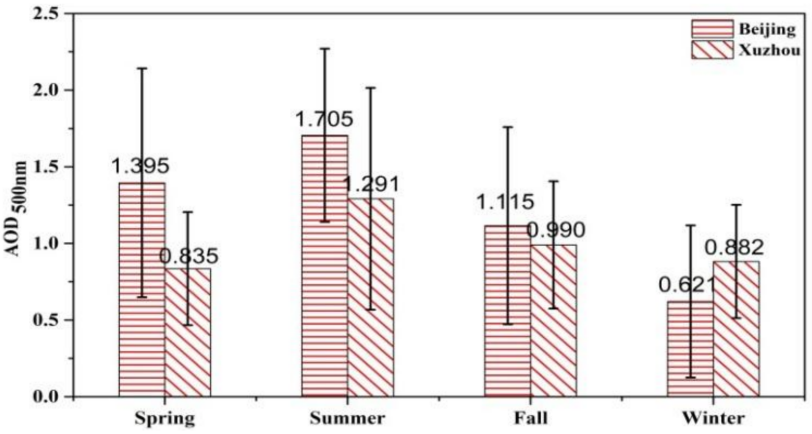

Figure 5. Seasonal averaged AOD at 500 nm on HPDs in Beijing and Xuzhou between 2013 and 2016.

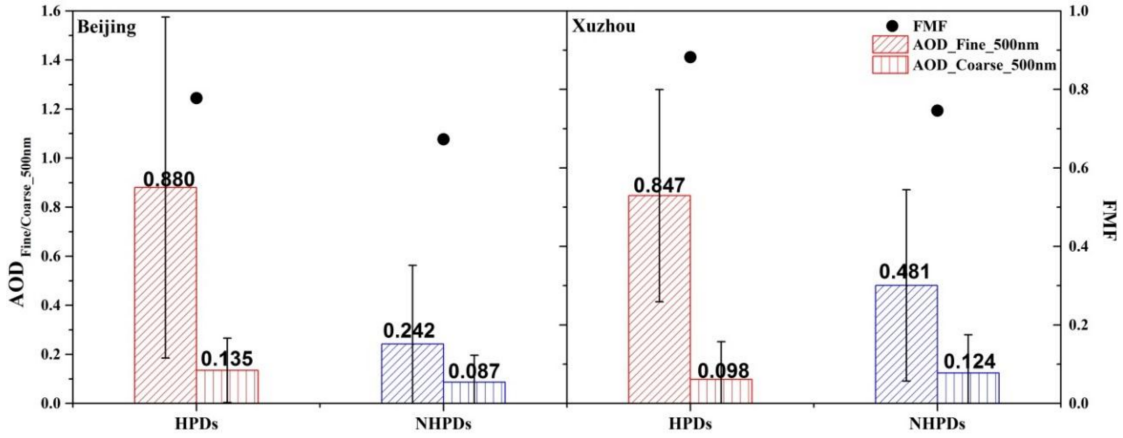

Figure 6. Averaged fine and coarse modes AOD at 500 nm and fine-mode fraction on HPDs and NHPDs between 2013 and 2016 in Beijing and Xuzhou, respectively.

As shown in Figure 7, the coarse mode $AOD_{500\,nm}$ was generally small and nearly constant both on HPDs and NHPDs. But the fine mode $AOD_{500\,nm}$ showed a dramatic increase on HPDs in comparison to NHPDs. In spring, the coarse mode AOD was larger than those of other seasons because of the presence of dust events. In summer, the coarse mode AOD was smallest as a result of the elimination of larger particles from frequent summer rainfall. Similarly, the fine mode AOD was largest as it closely related to hygroscopic growth of fine particles and gas-particle transformation.

The frequency distributions of α at 440–870 nm on HPDs from 2013 to 2016 in Beijing and Xuzhou are given in Figure 8. At both sites, the frequency histogram of α presents a uni-modal structure centered at 1.2–1.4. But the range of α in Beijing was markedly wider than that over Xuzhou. For $\alpha < 1.0$ and $\alpha > 1.0$, the relative frequencies in Beijing were 26.05% and 73.95%, respectively; while those in Xuzhou were 5.81% and 94.19%, respectively. A higher percentage of small α, together with a higher coarse mode AOD in Beijing, suggest that haze pollutions were more susceptible to coarse dust particles than Xuzhou.

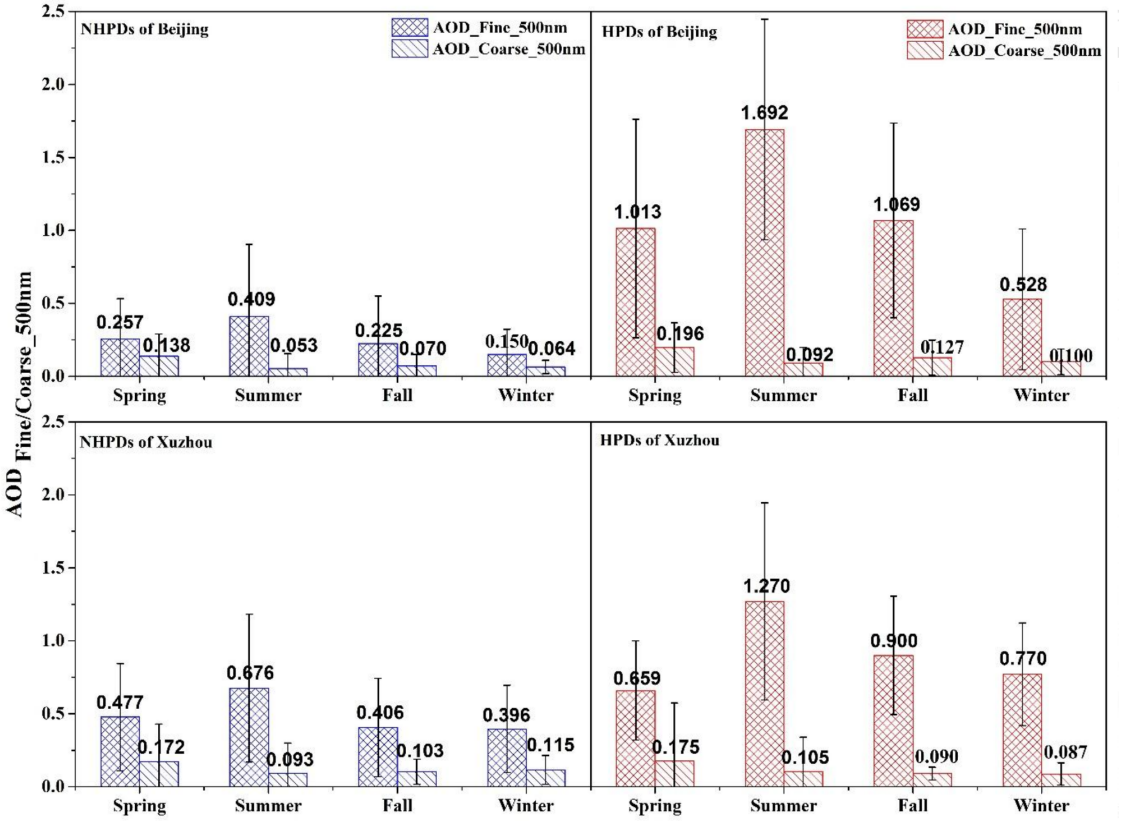

Figure 7. Seasonally averaged fine and coarse modes AOD at 500 nm between 2013 and 2016 on HPDs and NHPDs in Beijing and Xuzhou, respectively.

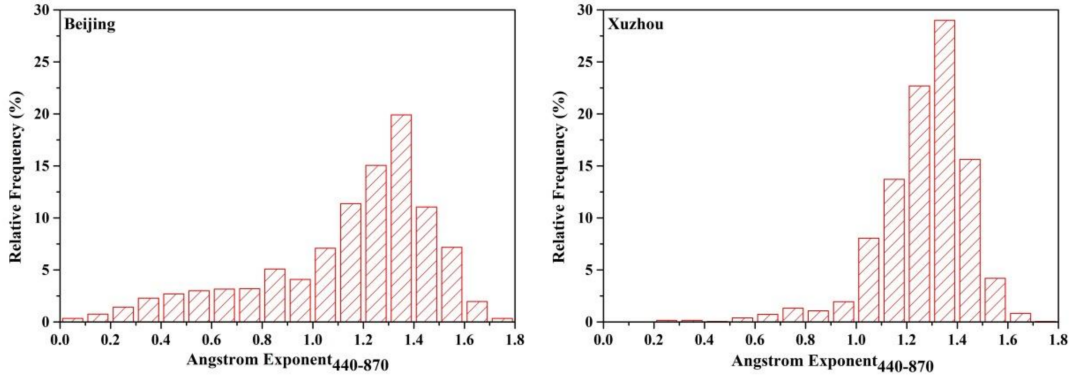

Figure 8. Frequency distributions of α at 440–870 nm on HPDs between 2013 and 2016 in Beijing and Xuzhou, respectively.

3.3. Size Distribution

The aerosol volume size distribution (dV(r)/dln(r)) was retrieved between 0.05 μm and 15 μm using AERONET inversion methodology. Figure 9 expresses the mean values of the dV(r)/dln(r) on HPDs and NHPDs at the two sites. They exhibit an obvious bimodal pattern with two peak radiuses in fine and coarse modes. In Beijing, the volume concentrations dramatically increased on HPDs in comparison to NHPDs in terms of both fine and coarse mode particles (~167% and ~80%, respectively). In Xuzhou, the volume concentration in fine mode showed an approximate 20% increase on HPDs in contrast to NHPDs, but the volume concentration in coarse mode remained relatively constant between HPDs and NHPDs. This is similar to the analysis of fine and coarse modes AOD in Figure 6. The particle size distribution in terms of matter concentration (particles per liter) from 0.25 μm to 32 μm in Xuzhou is presented in Figure 10. More than 99% particles fell within the scope of 0.25 μm to 0.7 μm. The total matter concentrations on HPDs were about three times greater than those on NHPDs.

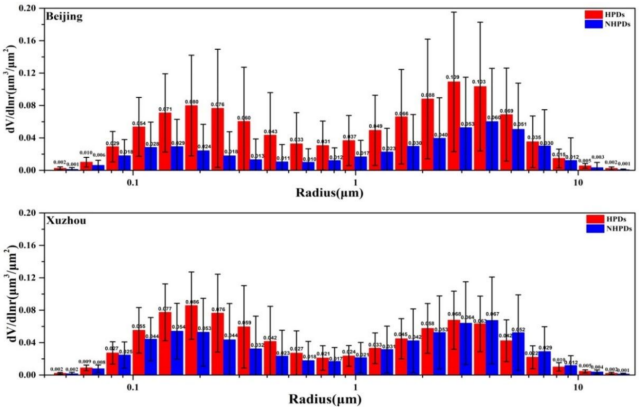

Figure 9. Averaged volume particle size distribution (dV(r)/dln(r)) on HPDs and NHPDs between 2013 and 2016 in Beijing and Xuzhou, respectively.

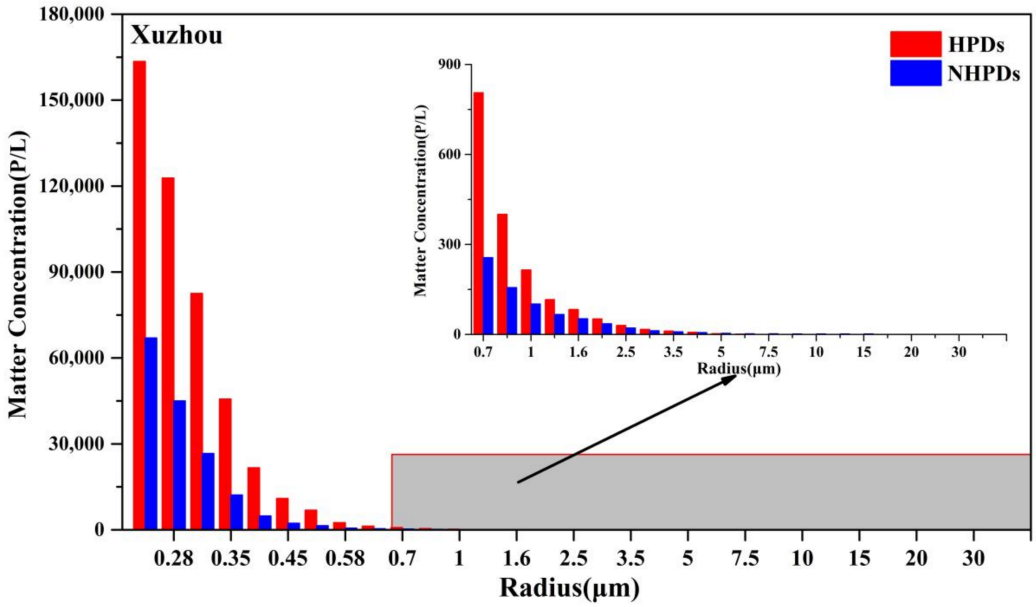

Figure 10. Averaged particle size distribution from Grimm 180 aerosol particle analyzer on HPDs and NHPDs between 2013 and 2016 in Xuzhou.

The seasonal variability in the dV(r)/dln(r) on HPDs at the two sites is compared in Figure 11. In Beijing, the fine mode showed the maxima peak at radius between 0.255 μm and 0.335 μm in summer,

and the coarse mode showed the maxima peak at a radius of 2.94 μm in spring. In Xuzhou, the fine mode showed the maxima peak at a radius of 0.335 μm in summer, but the differences of coarse mode were not significant among the four seasons. In both Beijing and Xuzhou, the largest volume concentration and radius in fine mode occurred in summer. This could be due to hygroscopic growth of fine particles with high relative humidity. The relative humidity data in Xuzhou from August 2014 to December 2016 exhibited a larger mean value of 75% in summer with an average of 67% for the rest of the year.

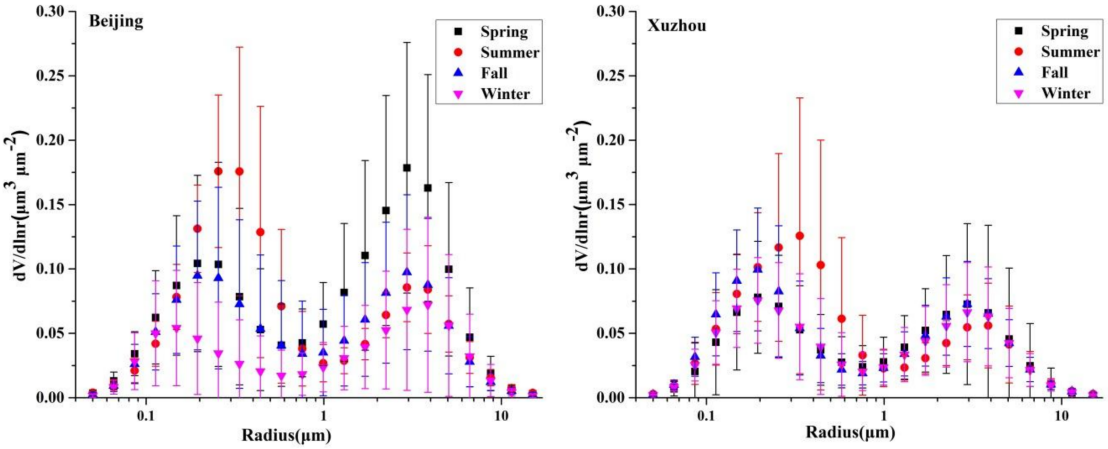

Figure 11. Seasonal averaged volume particle size distribution (dV(r)/dln(r)) on HPDs between 2013 and 2016 in Beijing and Xuzhou, respectively.

3.4. Single Scattering Albedo and Complex Refractive Index

The SSA is defined as the ratio of light scattering to total extinction due to aerosols; this is largely dependent on aerosol size, concentration of absorbing component, and its mixture state with non-absorbing components. Figure 12 presents the mean values of SSA at four wavelengths on HPDs and NHPDs in Beijing and Xuzhou from 2013 to 2016. In Beijing, the SSA values (0.874–0.897) on HPDs were much larger than those (0.843–0.853) on NHPDs. The SSA values at 440, 675, 870, and 1020 nm were found to increase by 0.031, 0.043, 0.048, and 0.049. In Xuzhou, the SSA values on HPDs were only slightly higher than those on NHPDs. Both HPD and NHPD values were higher in Xuzhou than in Beijing, indicating a relatively stronger scattering in Xuzhou.

The SSA is a key parameter in determining aerosol models used in satellite aerosol retrieval. The accuracy differences among different Moderate Resolution Imaging Spectroradiometer (MODIS) AOD products are partly due to differences in the assumptions of aerosol models. Levy et al. [47] determined aerosol models using the climatology of AERONET sites and applied them to the MODIS aerosol retrievals over land. They defined a non-absorbing fine-dominated aerosol type in developed urban/industrial regions like eastern China, with a SSA of ~0.95. Our results provide a more reasonable prior knowledge of aerosol optical parameter for retrieving haze optical depth in China [48,49].

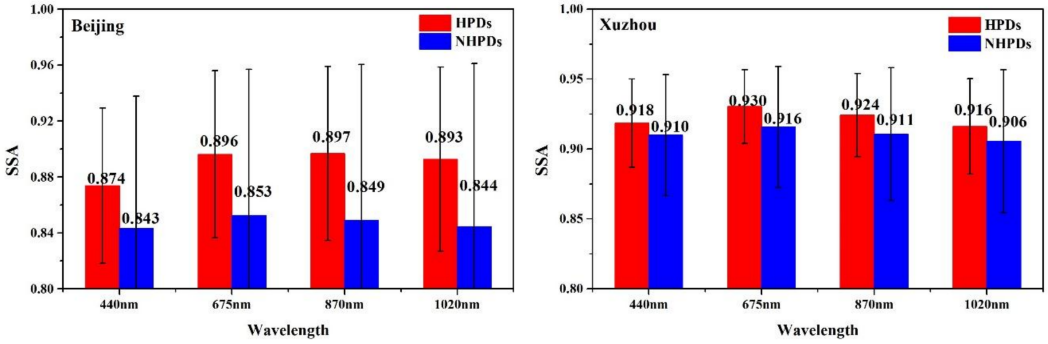

Figure 12. Averaged single scattering albedo (SSA) at four wavelengths on HPDs and NHPDs between 2013 and 2016 in Beijing and Xuzhou, respectively.

As shown in Figure 13, the seasonal characters of SSA were distinct with the largest value in summer and the smallest value in winter. The increase of water content led to the large SSA in summer and the small SSA could be attributed to an increase in absorbing black carbon aerosols during the heating period in winter. As the imaginary part of complex refractive index is an important parameter characterizing aerosol absorbing property, a uniform seasonal analysis was performed on the data and its results are presented in Figure 14. An opposite seasonal pattern of the imaginary part in comparison to the SSA was found. Between Beijing and Xuzhou, the differences in both SSA and the imaginary part were most noticeable in winter, especially at 440 nm. Low surface wind speed is one of the causes of Chinese haze pollution in winter [50], which is not favorable for aerosol mixing. Thus, the hazes are controlled by local-scale aerosol pollution and the difference in aerosol absorption properties between the two sites is the most significant.

The SSA and imaginary part exhibit different spectral behavior for different seasons, suggesting that there were several different aerosols types. Derimian et al. [51] employed the difference between the SSA at 440 nm and 1020 nm to distinguish between dust and black carbon. Negative values of the difference $SSA_{440\,nm}$–$SSA_{1020\,nm}$ will be related to stronger absorption by iron oxide in dust at 440 nm, while positive values are related to stronger absorption by black carbon at 1020 nm. In Figure 10, a positive value was only found in the summer in Xuzhou, which is connected to straw burning. Additionally, Kirchstetter et al. [52] found a relatively constant imaginary part for black carbon and a spectrally dependent imaginary part for organic carbon (specifically brown carbon). The spectral changes of the imaginary part in Figure 11 indicate the presence of brown carbon that is contributed to both by vehicular traffic and heavy industry.

Notably, the uncertainty of SSA will become much larger when $AOD_{440\,nm} < 0.4$ [33]. Hence, we provide the same analysis for SSA with $AOD_{440\,nm} \geq 0.4$ in Figures S1 and S2 (see Supplementary Materials). Similar characters of seasonal and spectral changes in SSA were seen.

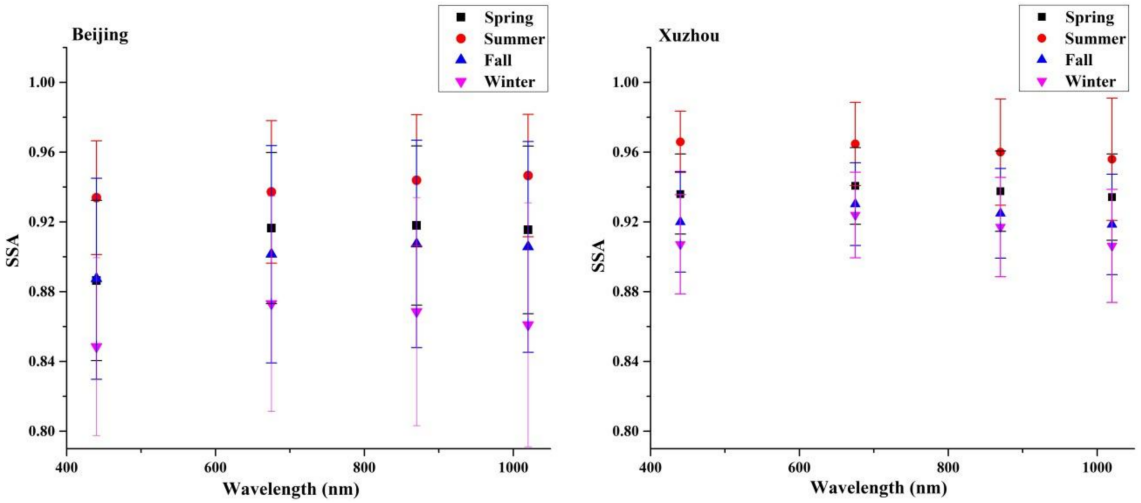

Figure 13. Seasonal averaged SSA at four wavelengths on HPDs between 2013 and 2016 in Beijing and Xuzhou, respectively.

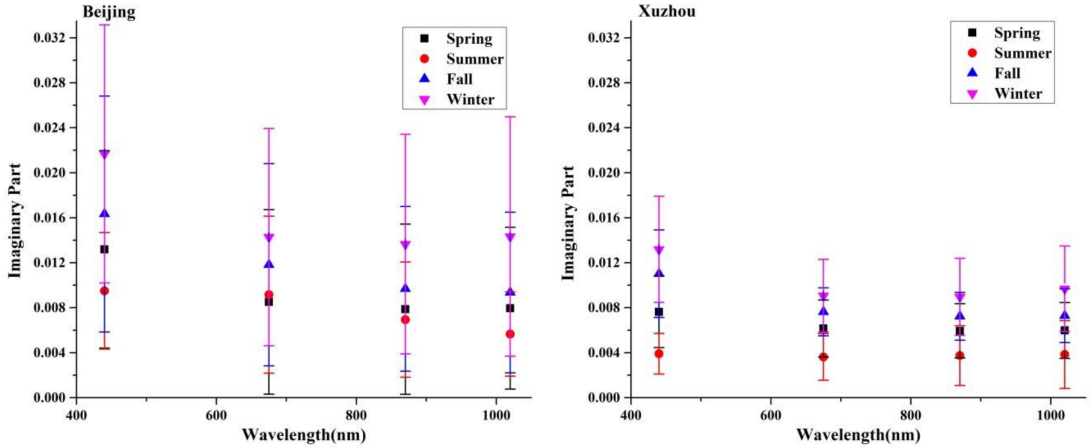

Figure 14. Seasonal averaged imaginary part of complex refractive index at four wavelengths on HPDs between 2013 and 2016 in Beijing and Xuzhou, respectively.

3.5. Aerosol Radiative Forcing

Based on the AERONET-retrieved aerosol optical properties, the SBDART was used to simulate the DARF. The comparison between the SBDART-simulated and AERONET-retrieved DARF shows good agreements with high correlation coefficients (averaged $R^2 > 0.93$, Figure S3 in the Supplementary Materials), indicating that the main input parameters were appropriate.

Figure 15 illustrates the averaged DARF values at the surface, top of atmosphere (TOA), and within the atmosphere on HPDs and NHPDs from 2013 to 2016 in Beijing and Xuzhou. The DARF values within the atmosphere were obtained from the DARF at the TOA minus those at surface. The mean DARF values were slightly negative at the TOA but were strongly negative at the surface. Accordingly, the DARF values within the atmosphere were moderately positive, suggesting a heating effect, as a significant amount of energy was trapped inside the atmosphere [53]. Such a heating effect was more than two times stronger on HPDs than NHPDs in Beijing, while the corresponding values between HPDs and NHPDs were close in Xuzhou. In comparison to the DARF, Figure 16 shows an opposite pattern of averaged radiative forcing efficiency (ARFE), defined as the forcing per unit optical depth, in this case, larger values on NHPDs and smaller ones on the HPDs. These results are consistent with a low AOD which could present a more significant impact on radiative forcing efficiencies [27,54,55].

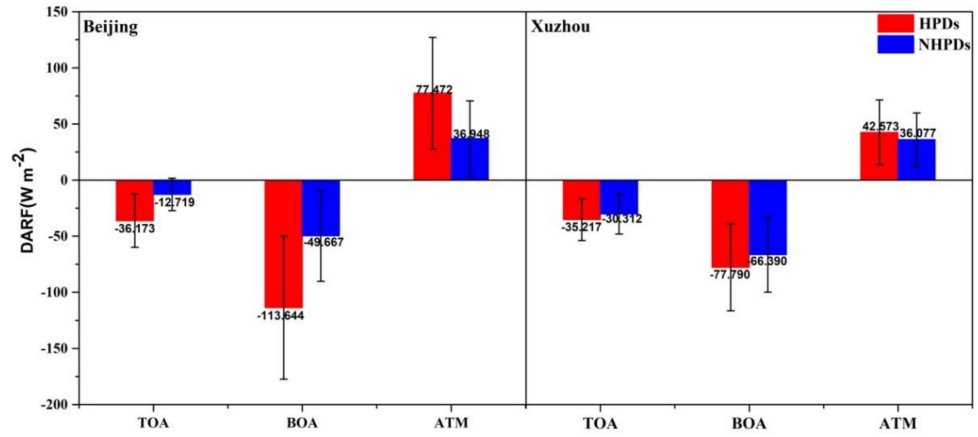

Figure 15. Averaged values of DARF at the surface (bottom of atmosphere, BOA), top of atmosphere (TOA) and within the atmosphere (ATM) on HPDs and NHPDs between 2013 and 2016 in Beijing and Xuzhou, respectively.

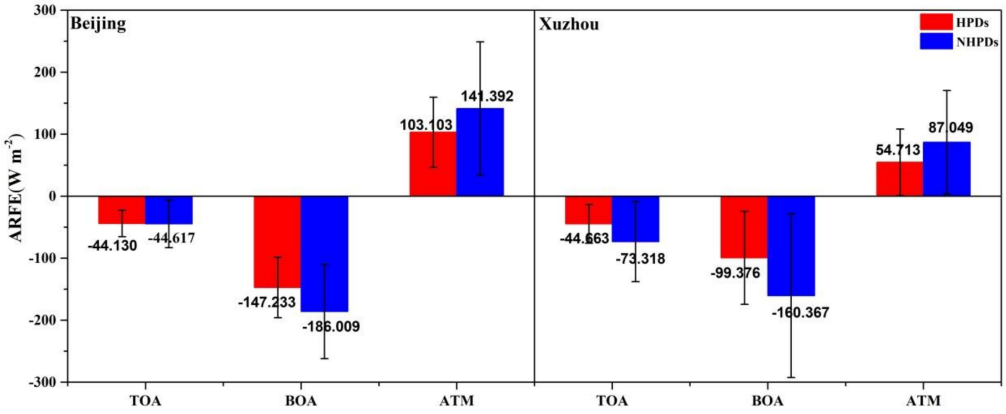

Figure 16. Averaged values of radiative forcing efficiency (ARFE) at the surface (bottom of atmosphere, BOA), top of atmosphere (TOA) and within the atmosphere (ATM) on HPDs and NHPDs between 2013 and 2016 in Beijing and Xuzhou, respectively.

The seasonal averaged values of DARF on HPDs are shown in Figure 17. The largest negative DARF at the surface and positive DARF within the atmosphere were found in spring and in fall respectively for Beijing and Xuzhou, implying strongest levels of cooling at the surface and warming in the atmosphere. For example, in Beijing the values were -80.6 ± 48.3 W/m^2 at the surface and -25.1 ± 17.9 W/m^2 at the TOA. These values are close to the case of common hazy days in the winter from late 2015 to early 2016 in Wuhan [30], but two to three times larger than January 2013 in Beijing [24].

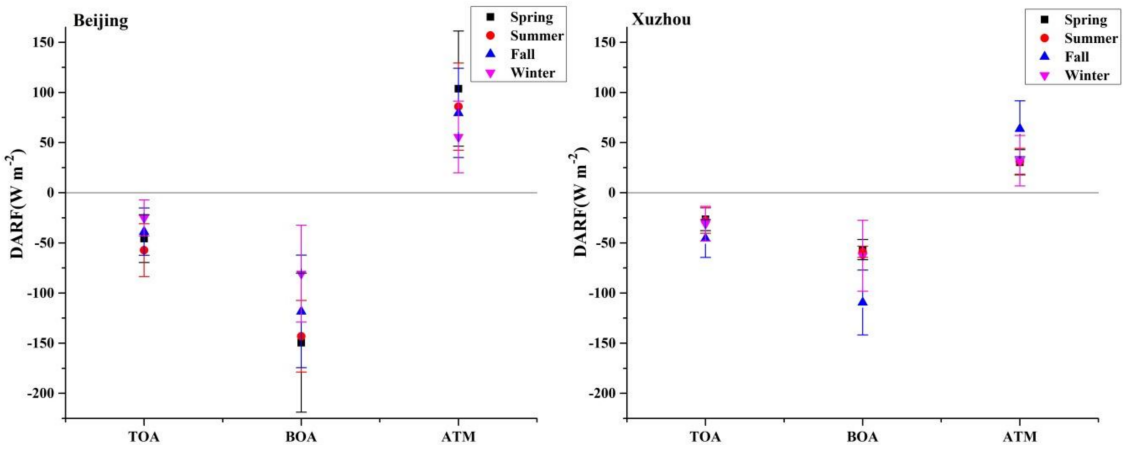

Figure 17. Seasonal averaged values of DARF in the surface (bottom of atmosphere, BOA), top of atmosphere (TOA) and within the atmosphere (ATM) on HPDs between 2013 and 2016 in Beijing and Xuzhou, respectively.

4. Conclusions

Aerosol optical properties during haze and non-haze pollution days were investigated at two AERONET urban sites in China (Beijing and Xuzhou) from January/July 2013 to December 2016. In addition, corresponding aerosol radiative forcing was estimated using the SBDART radiative transfer model. The major findings of this work are summarized as follows:

1. Haze pollution days accounted for 26% and 20% of all days from 2013 to 2016 in Beijing and Xuzhou, respectively, with the highest proportions in winter. The mean magnitudes of AOD at 550 nm on haze days were about 3.7 and 1.6 times greater than those on clean days in Beijing and Xuzhou, respectively. At both sites, the maximum AOD occurred in summer.
2. Haze pollutions were dominated by fine particles at both sites. However, in comparison to Xuzhou, Beijing had larger coarse mode AOD and a higher percentage of small α. These, together with the analysis of size distribution, suggested that the haze pollutions in Beijing were more susceptible to coarse dust particles than Xuzhou.
3. In Beijing, the values of SSA on haze pollution days greatly increase in comparison to clean days; however, this increase was much less evident in Xuzhou. The most noticeable differences in SSA and the imaginary part of complex refractive index between Beijing and Xuzhou were found in winter. The spectral changes in SSA for different seasons at both sites showed a larger $SSA_{440\,nm}$ than $SSA_{1020\,nm}$ during summer in Xuzhou, which is related to black carbon aerosols during straw burning episodes.
4. During haze days in Beijing, the mean values of DARF at the surface were -113.6 ± 63.7 W/m^2 and -36.2 ± 23.7 W/m^2 at the TOA. This produced an averaged heating effect of 77.5 ± 49.7 W/m^2 in the atmosphere that was more than two times stronger than clean days. In Xuzhou, the values of DARF appeared to be much smaller and the difference between haze and clean days was insignificant. The winter-averaged DARF on HPDs in Beijing were two to three times larger than January 2013 in Beijing.

These findings, derived from long-term ground-based observations, are more significant than previous short-term case studies (less than one month of data) for improving our understanding of haze formation in China and for assessing its impact on climate radiative effect. Further efforts should be dedicated to applying these findings to satellite aerosol retrievals under haze conditions.

Supplementary Materials: The following are available online at http://www.mdpi.com/2072-4292/10/4/518/s1. Figure S1: Averaged SSA with $AOD_{440\,nm} > 0.4$ on HPDs and NHPDs in Beijing and Xuzhou, Figure S2:

Seasonally averaged SSA with $AOD_{440\ nm} > 0.4$ on HPDs in Beijing and Xuzhou, Figure S3: Comparison between SBDART-simulated and AERONET-retrieved direct aerosol radiative forcing.

Acknowledgments: This study was supported by the Fundamental Research Funds for the Central Universities (2015XKMS049) and National Natural Science Foundation of China (Grant ID 41730109). We acknowledge financial support from the Jiangsu dual creative team programme project awarded to CUMT in 2017. We thank the GSFC/NASA AERONET group for processing the AERONET data and thank the principal investigators at Beijing-RADI site together with their staff for establishing and maintaining the instruments.

Author Contributions: Kai Qin and Luyao Wang wrote the article; Kai Qin conceived the idea; Letu Husi, Jian Xu and Kefei Zhang provided recommendation; Ding Li, Jiaheng Zou and Wenzhi Fan helped perform the statistical analysis.

Conflicts of Interest: The authors declare no conflict of interest.

Abbreviations

The following abbreviations are frequently used in this manuscript:

AOD	Aerosol Optical Depth
ARFE	Averaged Radiative Forcing Efficiency
AERONET	AErosol RObotic NETwork
BOA	Bottom of Atmosphere
dV(r)/dln(r)	Volume Size Distribution
DARF	Direct Aerosol Radiative Forcing
HPDs	Haze Pollution Days
NHPDs	Non-haze Pollution Days
SSA	Single Scattering Albedo
SBDART	Santa Barbara DISORT Atmospheric Radiative Transfer
TOA	Top of Atmosphere

References

1. Levy, H.I.; Horowitz, L.W.; Schwarzkopf, M.D.; Ming, Y.; Golaz, J.; Naik, V.; Ramaswamy, V. The roles of aerosol direct and indirect effects in past and future climate change. *J. Geophys. Res.* **2013**, *118*, 4521–4532. [CrossRef]
2. Liu, Y.; Diner, D.J. Multi-Angle Imager for Aerosols: A Satellite Investigation to Benefit Public Health. *Public Health Rep.* **2017**, *132*, 14–17. [CrossRef] [PubMed]
3. Holben, B.N.; Eck, T.F.; Slutsker, I. AERONET—A federated instrument network and data archive for aerosol characterization. *Remote Sens. Environ.* **1998**, *66*, 1–16. [CrossRef]
4. Goloub, P.; Li, Z.; Dubovik, O.; Blarel, L.; Podvin, T.; Jankowiak, I.; Lecoq, R.; Lecoq, R.; Deroo, C.; Chatenet, B.; et al. PHOTONS/AERONET Sunphotometer Network Overview: Description, Activities, Results. *Proc. SPIE* **2008**, *6936*. [CrossRef]
5. Che, H.; Xia, X.; Zhu, J.; Wang, H.; Wang, Y.; Sun, J.; Zhang, X.; Shi, G. Aerosol optical properties under the condition of heavy haze over an urban site of Beijing, China. *Environ. Sci. Pollut. Res.* **2015**, *22*, 1043–1053. [CrossRef] [PubMed]
6. Khatri, P.; Takamura, T.; Nakajima, T.; Estelles, V.; Irie, H.; Kuze, H.; Campanelli, M.; Sinyuk, A.; Lee, S.M.; Sohn, B.J.; et al. Factors for inconsistent aerosol single scattering albedo between SKYNET and AERONET. *J. Geophys. Res.* **2016**, *121*, 1859–1877. [CrossRef]
7. Pandithurai, G.; Pinker, R.T.; Takamura, T.; Devara, P. Aerosol radiative forcing over a tropical urban site in India. *Geophys. Res. Lett.* **2004**, *31*, L1210712. [CrossRef]
8. Eck, T.F.; Holben, B.N.; Dubovik, O.; Smirnov, A.; Goloub, P.; Chen, H.B.; Chatenet, B.; Gomes, L.; Zhang, X.Y.; Tsay, S.C.; et al. Columnar aerosol optical properties at AERONET sites in central eastern Asia and aerosol transport to the tropical mid-Pacific. *J. Geophys. Res.* **2005**, *110*, D6202. [CrossRef]
9. Lyamani, H.; Olmo, F.J.; Alados-Arboledas, L. Physical and optical properties of aerosols over an urban location in Spain: Seasonal and diurnal variability. *Atmos. Chem. Phys.* **2010**, *10*, 239–254. [CrossRef]
10. Alam, K.; Trautmann, T.; Blaschke, T.; Majid, H. Aerosol optical and radiative properties during summer and winter seasons over Lahore and Karachi. *Atmos. Environ.* **2012**, *50*, 234–245. [CrossRef]

11. Valenzuela, A.; Olmo, F.J.; Lyamani, H.; Anton, M.; Quirantes, A.; Alados-Arboledas, L. Aerosol radiative forcing during African desert dust events (2005–2010) over Southeastern Spain. *Atmos. Chem. Phys.* **2012**, *12*, 10331–10351. [CrossRef]
12. Chatterjee, A.; Ghosh, S.K.; Adak, A.; Singh, A.K.; Devara, P.C.S.; Raha, S. Effect of Dust and Anthropogenic Aerosols on Columnar Aerosol Optical Properties over Darjeeling (2200 m asl), Eastern Himalayas, India. *PLoS ONE* **2012**, *7*, e402867. [CrossRef] [PubMed]
13. Adesina, A.J.; Kumar, K.R.; Sivakumar, V.; Griffith, D. Direct radiative forcing of urban aerosols over Pretoria (25.75 degrees S, 28.28 degrees E) using AERONET Sunphotometer data: First scientific results and environmental impact. *J. Environ. Sci.* **2014**, *26*, 2459–2474. [CrossRef] [PubMed]
14. Tao, R.; Che, H.; Chen, Q.; Tao, J.; Wang, Y.; Sun, J.; Wang, H.; Zhang, X. Study of Aerosol Optical Properties Based on Ground Measurements over Sichuan Basin, China. *Aerosol Air Qual. Res.* **2014**, *14*, 905–915. [CrossRef]
15. Kaskaoutis, D.G.; Sinha, P.R.; Vinoj, V.; Kosmopoulos, P.G.; Tripathi, S.N.; Misra, A.; Sharma, M.; Singh, R.P. Aerosol properties and radiative forcing over Kanpur during severe aerosol loading conditions. *Atmos. Environ.* **2013**, *79*, 7–19. [CrossRef]
16. Jose, S.; Gharai, B.; Niranjan, K.; Rao, P.V.N. Investigation on seasonal variations of aerosol properties and its influence on radiative effect over an urban location in central India. *Atmos. Environ.* **2016**, *133*, 41–48. [CrossRef]
17. Gharibzadeh, M.; Alam, K.; Bidokhti, A.A.; Abedini, Y.; Masoumi, A. Radiative Effects and Optical Properties of Aerosol during Two Dust Events in 2013 over Zanjan, Iran. *Aerosol Air Qual. Res.* **2017**, *17*, 888–898. [CrossRef]
18. Li, S.; Ma, Z.; Xiong, X.; Christiani, D.C.; Wang, Z.; Liu, Y. Satellite and Ground Observations of Severe Air Pollution Episodes in the Winter of 2013 in Beijing, China. *Aerosol Air Qual. Res.* **2016**, *16*, 977–989. [CrossRef]
19. Shang, H.; Chen, L.; Letu, H.; Zhao, M.; Li, S.; Bao, S. Development of a daytime cloud and haze detection algorithm for Himawari-8 satellite measurements over central and eastern China. *J. Geophys. Res.* **2017**, *122*, 3528–3543. [CrossRef]
20. Guo, J.P.; He, J.; Liu, H.L.; Miao, Y.C.; Liu, H.; Zhai, P.M. Impact of various emission control schemes on air quality using WRF-Chem during APEC China 2014. *Atmos. Environ.* **2016**, *140*, 311–319. [CrossRef]
21. Qin, K.; Rao, L.; Xu, J.; Bai, Y.; Zou, J.; Hao, N.; Li, S.; Yu, C. Estimating ground level NO_2 concentrations over central-eastern china using a satellite-based geographically and temporally weighted regression model. *Remote Sens.* **2017**, *9*, 950. [CrossRef]
22. Qin, K.; Wu, L.; Wong, M.S.; Letu, H.; Hu, M.; Lang, H.; Sheng, S.; Teng, J.; Xiao, X.; Yuan, L. Trans-boundary aerosol transport during a winter haze episode in China revealed by ground-based Lidar and CALIPSO satellite. *Atmos. Environ.* **2016**, *141*, 20–29. [CrossRef]
23. Li, Z.; Gu, X.; Wang, L.; Li, D.; Xie, Y.; Li, K.; Dubovik, O.; Schuster, G.; Goloub, P.; Zhang, Y.; et al. Aerosol physical and chemical properties retrieved from ground-based remote sensing measurements during heavy haze days in Beijing winter. *Atmos. Chem. Phys.* **2013**, *13*, 10171–10183. [CrossRef]
24. Bi, J.; Huang, J.; Hu, Z.; Holben, B.N.; Guo, Z. Investigating the aerosol optical and radiative characteristics of heavy haze episodes in Beijing during January of 2013. *J. Geophys. Res.* **2014**, *119*, 9884–9900. [CrossRef]
25. Che, H.; Zhang, X.Y.; Xia, X.; Goloub, P.; Holben, B.; Zhao, H.; Wang, Y.; Zhang, X.C.; Wang, H.; Blarel, L.; et al. Ground-based aerosol climatology of China: Aerosol optical depths from the China Aerosol Remote Sensing Network (CARSNET) 2002–2013. *Atmos. Chem. Phys.* **2015**, *15*, 7619–7652. [CrossRef]
26. Yu, X.; Kumar, K.R.; Lu, R.; Ma, J. Changes in column aerosol optical properties during extreme haze-fog episodes in January 2013 over urban Beijing. *Environ. Pollut.* **2016**, *210*, 217–226. [CrossRef] [PubMed]
27. Che, H.; Xia, X.; Zhu, J.; Li, Z.; Dubovik, O.; Holben, B.; Goloub, P.; Chen, H.; Estelles, V.; Cuevas-Agullo, E.; et al. Column aerosol optical properties and aerosol radiative forcing during a serious haze-fog month over North China Plain in 2013 based on ground-based sunphotometer measurements. *Atmos. Chem. Phys.* **2014**, *14*, 2125–2138. [CrossRef]
28. Qin, K.; Wang, L.; Wu, L.; Xu, J.; Rao, L.; Letu, H.; Shi, T.W.; Wang, R.F. A campaign for investigating aerosol optical properties during winter hazes over Shijiazhuang, China. *Atmos. Res.* **2017**, *198*, 113–122. [CrossRef]
29. Kang, N.; Kumar, K.R.; Yu, X.; Yin, Y. Column-integrated aerosol optical properties and direct radiative forcing over the urban-industrial megacity Nanjing in the Yangtze River Delta, China. *Environ. Sci. Pollut. Res.* **2016**, *23*, 17532–17552. [CrossRef] [PubMed]

30. Zhang, M.; Ma, Y.; Gong, W.; Wang, L.; Xia, X.; Che, H.; Hu, B.; Liu, B. Aerosol radiative effect in UV, VIS, NIR, and SW spectra under haze and high-humidity urban conditions. *Atmos. Environ.* **2017**, *166*, 9–21. [CrossRef]
31. AERONET (Aerosol Robotic Network). Available online: http://aeronet.gsfc.nasa.gov (accessed on 26 December 2017).
32. SRTM 90m Digital Elevation Data. Available online: http://srtm.csi.cgiar.org/ (accessed on 15 March 2018).
33. Dubovik, O.; Smirnov, A.; Holben, B.N.; King, M.D.; Kaufman, Y.J.; Eck, T.F.; Slutsker, I. Accuracy assessments of aerosol optical properties retrieved from Aerosol Robotic Network (AERONET) Sun and sky radiance measurements. *J. Geophys. Res.* **2000**, *105*, 9791–9806. [CrossRef]
34. O'Neill, N.T.; Eck, T.F.; Smirnov, A.; Holben, B.N.; Thulasiraman, S. Spectral discrimination of coarse and fine mode optical depth. *J. Geophys. Res.* **2003**, *108*, 4559. [CrossRef]
35. Dubovik, O.; King, M.D. A flexible inversion algorithm for retrieval of aerosol optical properties from Sun and sky radiance measurements. *J. Geophys. Res.* **2000**, *105*, 20673–20696. [CrossRef]
36. Dubovik, O.; Holben, B.; Eck, T.F.; Smirnov, A.; Kaufman, Y.J.; King, M.D.; Tanre, D.; Slutsker, I. Variability of absorption and optical properties of key aerosol types observed in worldwide locations. *J. Atmos. Sci.* **2002**, *59*, 590–608. [CrossRef]
37. National Real-Time Air Quality Reporting System. Available online: http://106.37.208.233:20035/ (accessed on 26 December 2017).
38. Weather for 243 Countries of the World. Available online: https://rp5.ru/ (accessed on 26 December 2017).
39. Ricchiazzi, P.; Yang, S.; Gautier, C. SBDART: A research and teaching software tool for plane-parallel radiative transfer in the Earth's atmosphere. *Bull. Am. Meteorol. Soc.* **1998**, *79*, 2101–2114. [CrossRef]
40. NASA GES DISC. Available online: http://disc.sci.gsfc.nasa.gov/giovanni (accessed on 26 December 2017).
41. Halthore, R.N.; Crisp, D.; Schwartz, S.E.; Anderson, G.P.; Berk, A.; Bonnel, B.; Boucher, O.; Chang, F.L.; Chou, M.D.; Clothiaux, E.E.; et al. Intercomparison of shortwave radiative transfer codes and measurements. *J. Geophys. Res.* **2005**, *110*, D11206. [CrossRef]
42. Wu, Y.; Han, Y.; Voulgarakis, A.; Wang, T.; Li, M.; Wang, Y.; Xie, M.; Zhuang, B.; Li, S. An agricultural biomass burning episode in eastern China: Transport, optical properties, and impacts on regional air quality. *J. Geophys. Res.* **2017**, *122*, 2304–2324. [CrossRef]
43. Adeyewa, Z.D.; Balogun, E.E. Wavelength dependence of aerosol optical depth and the fit of the Angstrom law. *Theor. Appl. Climatol.* **2003**, *74*, 105–122. [CrossRef]
44. Wang, Z.; Liu, D.; Wang, Y.; Shi, G. Diurnal aerosol variations do affect daily averaged radiative forcing under heavy aerosol loading observed in Hefei, China. *Atmos. Meas. Tech.* **2015**, *8*, 2901–2907. [CrossRef]
45. Li, W.J.; Shao, L.Y.; Buseck, P.R. Haze types in Beijing and the influence of agricultural biomass burning. *Atmos. Chem. Phys.* **2010**, *10*, 8119–8130. [CrossRef]
46. Che, H.; Zhao, H.; Wu, Y.; Xia, X.; Zhu, J.; Wang, H.; Wang, Y.; Sun, J.; Yu, J.; Zhang, X.; et al. Analyses of aerosol optical properties and direct radiative forcing over urban and industrial regions in Northeast China. *Meteorol. Atmos. Phys.* **2015**, *127*, 345–354. [CrossRef]
47. Levy, R.C.; Remer, L.A.; Dubovik, O. Global aerosol optical properties and application to Moderate Resolution Imaging Spectroradiometer aerosol retrieval over land. *J. Geophys. Res. Atmos.* **2007**, *112*, D13210. [CrossRef]
48. Li, S.; Chen, L.; Xiong, X.; Tao, J.; Su, L.; Han, D.; Liu, Y. Retrieval of the haze optical thickness in North China Plain using MODIS data. *IEEE Trans. Geosci. Remote Sens.* **2013**, *51*, 2528–2540. [CrossRef]
49. Yan, X.; Shi, W.; Luo, N.; Zhao, W. A new method of satellite-based haze aerosol monitoring over the North China Plain and a comparison with MODIS Collection 6 aerosol products. *Atmos. Res.* **2016**, *171*, 31–40. [CrossRef]
50. Wang, L.; Gong, W.; Xia, X.; Zhu, J.; Li, J.; Zhu, Z. Long-term observations of aerosol optical properties at Wuhan, an urban site in Central China. *Atmos. Environ.* **2015**, *101*, 94–102. [CrossRef]
51. Derimian, Y.; Karnieli, A.; Kaufman, Y.J.; Andreae, M.O.; Andreae, T.W.; Dubovik, O.; Koren, I. The role of iron and black carbon in aerosol light absorption. *Atmos. Chem. Phys.* **2008**, *8*, 3623–3637. [CrossRef]
52. Kazadzis, S.; Kouremeti, N.; Bais, A.; Kazantzidis, A.; Meleti, C. Aerosol forcing efficiency in the UVA region from spectral solar irradiance measurements at an urban environment. *Ann. Geophys.* **2009**, *27*, 2515–2522. [CrossRef]
53. Esteve, A.R.; Estelles, V.; Utrillas, M.P.; Martinez-Lozano, J.A. Analysis of the aerosol radiative forcing over a Mediterranean urban coastal site. *Atmos. Res.* **2014**, *137*, 195–204. [CrossRef]

54. Xia, X.; Chen, H.; Goloub, P.; Zhang, W.; Chatenet, B.; Wang, P. A compilation of aerosol optical properties and calculation of direct radiative forcing over an urban region in northern China. *J. Geophys. Res.* **2007**, *112*, D12203. [CrossRef]
55. Chen, W.; Yan, L.; Ding, N.; Xie, M.; Lu, M.; Zhang, F.; Duan, Y.; Zong, S. Analysis of Aerosol Radiative Forcing over Beijing under Different Air Quality Conditions Using Ground-Based Sun-Photometers between 2013 and 2015. *Remote Sens.* **2016**, *8*, 510. [CrossRef]